Aerospace Systems
https://doi.org/10.1007/s42401-023-00243-4

ORIGINAL PAPER

Non-unique regimes of oscillatory transonic flow in bent channels

Alexander Kuzmin[1]

Received: 18 April 2023 / Revised: 21 June 2023 / Accepted: 25 July 2023

Abstract
The turbulent transonic two-dimensional airflow in 9°-bent channels is studied numerically on the basis of the Reynolds-averaged Navier–Stokes equations. The flow is supersonic at the entrance of channels and subsonic at the exit. Numerical solutions reveal non-uniqueness of flow regimes in certain ranges of boundary conditions. The location of a formed shock wave exhibits hysteresis with changes in the inflow Mach number M_∞, or the angle of attack, or pressure given at the exit p_{exit}. The existence of hysteresis is caused by an interaction of the shock wave with an expansion flow region over the convex wall of channel. Shock wave behavior under forced oscillations of the Mach number M_∞ or pressure p_{exit} is discussed. Dependencies of hysteresis and non-unique regimes on the amplitude and period of the oscillations of M_∞, p_{exit} are studied. It is shown that hysteresis in a long channel is essentially wider than that in a short one.

Keywords Turbulent flow · Numerical simulation · Shock waves · Oscillations · Hysteresis

1 Introduction

Studies of transonic flow in bent channels are of practical interest, e.g., for advanced design of mixed-compression and S-shaped intakes of air-breathing engines [1–3]. Also, transonic flow in curved channels is realized in so-called ram-pressors, which are compressors operating at high peripheral speeds [4, 5]. Meanwhile, the phenomenon of hysteresis in such flows remains insufficiently investigated.

Guo et al. [6] studied numerically 2D transonic flow in a curved channel of almost constant cross section and showed the existence of flow hysteresis with changes in the back-pressure given at the exit. Feng et al. [7, 8] investigated both experimentally and numerically the airflow in a curved channel that modeled a combustion chamber; they obtained hysteresis of static pressure on a wall of the channel with changes in the exit area.

Krushnarao Kotteda and Mittal [9] explored a slightly divergent Y-shaped intake at various backpressures and obtained different flow regimes as a result of these variations. Jin et al. [10] performed numerical and experimental study of flow hysteresis in a mixed-compression intake with variable throat geometry. It was suggested that the key factor affecting the hysteresis is the separation ahead of the inlet.

For an intake studied by Das and Prasad [2] and its modification, flow hysteresis with changes in the free-stream Mach number was demonstrated in Ref. [11, Fig. 7]. In a paper [12], Kuzmin examined transonic flow in a 9°-bent channel of constant cross-section areas before and after the bend. The study was focused on the interaction of an arising shock wave with an expansion flow region over the convex wall of channel. Numerical simulations showed that instability of the interaction causes hysteresis of shock locations with changes in the free-stream Mach number M_∞. In addition, computations revealed a double hysteresis (with three branches of the hysteresis curve) in narrow ranges of M_∞ at several angles of attack, free-stream pressures p_∞, and backpressures p_{exit}. The airflow in a similar channel whose convex wall is slightly shifted downstream was studied in Ref. [13]. In this case, the double hysteresis changes for conventional one; at the same time, computations showed a double hysteresis with variation of p_{exit} for a modified channel whose convex corner is smoothed with a circular arc of radius $R = 101.6$ mm or $R = 190.6$ mm.

In the present paper, we first consider the same channel with $R = 190.6$ mm as the one explored in Ref. [13] and demonstrate a double hysteresis with variation of free-stream Mach number M_∞ or angle of attack α instead of p_{exit}. Then,

✉ Alexander Kuzmin
a.kuzmin@spbu.ru

[1] Department of Fluid Dynamics, St. Petersburg State University, St. Petersburg, Russia

Published online: 07 August 2023

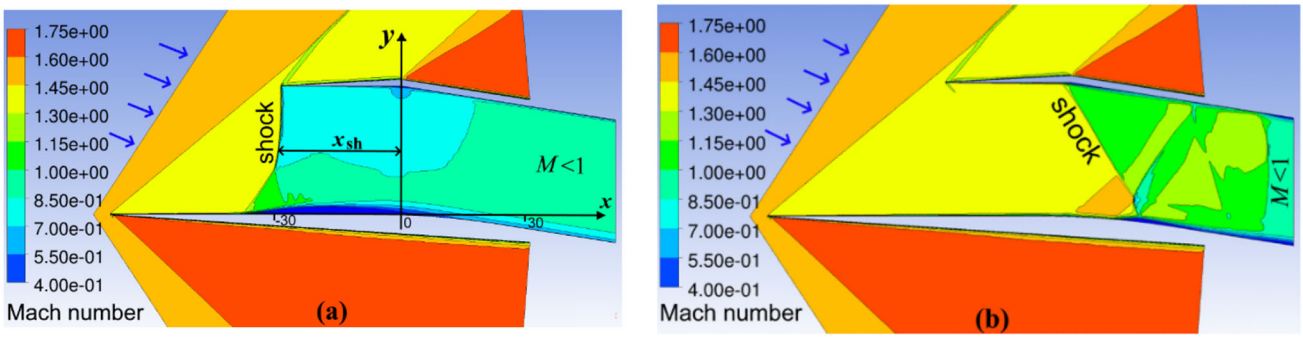

Fig. 1 Channel A: Mach number contours at $M_\infty = 1.59$, $p_{\text{exit}} = 1.82 \times 10^5$ Pa in different regimes, in which the shock wave is located **a** at the entrance, **b** near the bend of channel

we impose an oscillating Mach number $M_\infty(t)$ or backpressure $p_{\text{exit}}(t)$ and study flow regimes at several amplitudes and periods of oscillations. Finally, transonic flow hysteresis in a longer channel is examined. We mention that fluctuations in free-stream Mach number occur in practice during a vehicle flight in turbulent atmosphere, whereas unsteady backpressures may arise in air intake due to instability of fuel burning in the engine.

2 Formulation of the problem and numerical method

Figure 1 shows a fragment of the airflow and walls of Channel A. Here and further in the paper, the Cartesian coordinates (x, y) and sizes of the channels are dimensional and given in millimeters. Inner surfaces of the upper and lower walls are 9°-bent. The heights of the vertical sections before and after the bend are $h_1 = 30$ and $h_2 = 28.8$, respectively. The lower wall corner is smoothed with a circular arc of radius $R = 190.6$. Leading edges of the upper and lower walls are located at $x = -28$ and $x = -68$, respectively, where initial thickness of walls is 0.05. The exit section of Channel A is set at $x = 50$. Further details of the channel geometry and outer boundaries of the computational domain are available in Ref. [13]. In Sect. 3.3, we will study flow regimes in a longer Channel B obtained by a straight prolongation of the upper and lower walls of Channel A from $x = 50$ to $x = 130$.

On the inflow boundary Γ_{in} of computational domain (see Fig. 2), we set the static pressure $p_\infty = 8 \times 10^4$ N/m^2, angle of attack α, the x- and y-components $U_\infty = M_\infty a_\infty \cos\alpha$, $V_\infty = M_\infty a_\infty \sin\alpha$ of flow velocity, the turbulence level of 1%, and static temperature $T_\infty = 200$ K which determines the sound speed $a_\infty = 283.58$ m/s. We set $\alpha = -5°$ throughout the paper, except for Fig. 5 which shows a shock wave coordinate as a function of α. The Reynolds number based on the height h_1 of channel and $M_\infty = 1.6$ is 5.75×10^5.

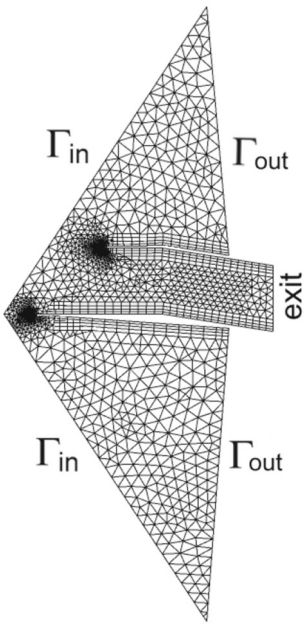

Fig. 2 Schematic of the computational domain and mesh

At the exit of channel, we impose the static pressure p_{exit} and condition of subsonic flow. On the outflow boundary Γ_{out} of the computational domain outside of channel, we prescribe the condition of supersonic flow. The adiabatic and no-slip conditions are imposed on the walls. Initial data are determined by the free stream or a flow field obtained for other values of M_∞, p_{exit}, α.

The air is assumed to be a perfect gas whose molar mass is 28.96 kg/kmol, the ratio of specific heats is 1.4, and specific heat at constant pressure is 1004.4 J/(kg K). For the molecular dynamic viscosity we use the Sutherland formula.

Numerical simulations were based on the system of unsteady Reynolds-averaged Navier–Stokes equations [14] with respect to static pressure $p(x, y, t)$, temperature $T(x, y, t)$, and velocity components $U(x, y, t)$, $V(x, y, t)$. Solutions

of the equations were obtained with an ANSYS-18.2 CFX finite-volume solver [15] using a high-resolution scheme for convective terms and a shear stress transport k-ω turbulence model [16]. An implicit backward Euler scheme was employed for advancing in time t.

Flow simulations were performed on a hybrid unstructured grid constituted by quadrangles in 40 layers on the walls and by triangles in the remaining region. The non-dimensional thickness y^+ of the first mesh layer on the walls was less than 1.2. The total number of grid cells was 641,879. The global timestep of 10^{-6} s ensured the root-mean-square Courant–Friedrichs–Lewy number smaller than 2. Test computations on a refined grid of approximately 1.3×10^9 cells only showed insignificant changes (less than 1.3%) in shock wave coordinates. In addition, our simulation of a benchmark problem for a supersonic intake demonstrated good agreement with numerical and experimental data available in the literature [11, Fig. 3].

3 Results and discussion

3.1 Flow hysteresis in Channel A at steady boundary conditions

At steady boundary conditions, numerical solutions of the initial-boundary value problem demonstrated a convergence of the mean parameters p, ρ, U, V, T of turbulent flow to steady states. The solutions reveal flow hysteresis and non-uniqueness in narrow bands of the boundary parameters; the realization of a certain steady regime depends on initial conditions. For example, Fig. 1a and b depicts two different flows obtained at $M_\infty = 1.59$ using initial data which had been computed in advance at $M_\infty = 1.58$ and $M_\infty = 1.60$, respectively. As seen, the arisen shock wave is located at the entrance in Fig. 1a and near the bend of channel in Fig. 1b.

In what follows, we will trace the longitudinal location of the shock wave using its x-coordinate x_{sh} at the height $y = 15$, see Fig. 1a. The obtained values of x_{sh} with step-by-step variation of M_∞ at three backpressures are depicted in Fig. 3. In each case, computations started at maximum Mach numbers, which correspond to the right endpoints of the shown curves. For example, to obtain the upper branch of curve 1 (located at the height $x_{sh} \approx 7$), the flow field was computed step-by-step at decreasing M_∞ from 1.595 to 1.585, and values of x_{sh} were documented at each step. In this regime, the main shock wave is located near the bend of channel (swallowed shock) and the flow is supersonic in a major part of channel, see Fig. 4a.

Further decrease of M_∞ to 1.584 results in a drop of the shock coordinate x_{sh} from 7.1 to 2.3 and an abrupt shrinking of the supersonic region, see Fig. 4b. This is associated with an upstream shift of the region where boundary layer

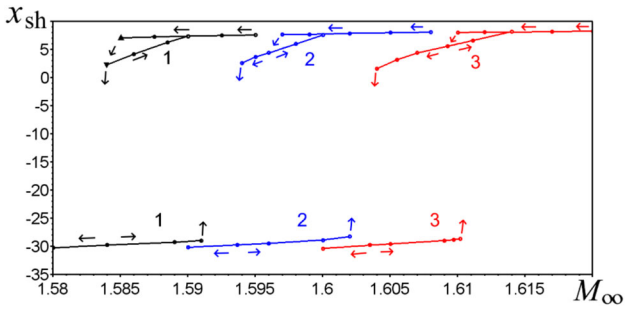

Fig. 3 Channel A: coordinate x_{sh} of shock wave as a function of the Mach number M_∞ at three backpressures: 1—$p_{exit} = 1.82 \times 10^5$ Pa, 2—$p_{exit} = 1.87 \times 10^5$ Pa, 3—$p_{exit} = 1.92 \times 10^5$ Pa. The upper (lower) branches of the curves correspond to flow regimes with a swallowed (expelled) shock wave

is separated from the lower wall. After that, a step-by-step increase in M_∞ to 1.590 produces a gradual expansion of the supersonic region downstream of the bend, and a rise of x_{sh} as illustrated by the second upper branch of curve 1 (which is located at heights between $x_{sh} = 2.3$ and $x_{sh} = 7.4$).

If M_∞ decreases to smaller values than 1.584, then the shock jumps further upstream, and flow relaxation yields a regime with the shock located near the entrance of channel (expelled shock). The coordinate x_{sh} drops to values about -30, and after that further variations of M_∞ in both directions produce the lower branch of curve 1.

Thus, the principal hysteresis is created by transitions between the upper and lower branches of the curves as indicated by arrows in Fig. 3. These transitions are caused by the shock wave interaction with an expansion flow region over the bend of lower wall. The interaction produces a rupture/coalescence of supersonic regions at the bend of channel and jumps of the shock. The width of principal hysteresis depends on the size of supersonic region developed downstream of the bend [12, Figs. 5, 6]. This kind of hysteresis occurs in both turbulent and inviscid flows.

Two upper branches of curves in Fig. 3 create a minor hysteresis in the regime with a swallowed shock. This is caused by different locations of the boundary layer separation with increasing and decreasing M_∞. We notice that flow hysteresis associated with boundary layer separation was observed in straight channels as well [17, 18].

Figure 5 exhibits a double hysteresis obtained with step-by-step variation of the angle of attack α.

Computations showed that the smoothing of the upper wall corner with an arc of sufficiently small radius R only insignificantly changes the flow behavior. Meanwhile if the radius R is large enough, e.g., the same as the one smoothing the lower corner, then computations demonstrate a conventional hysteresis in the dependence $x_{sh}(M_\infty)$ instead of the double one.

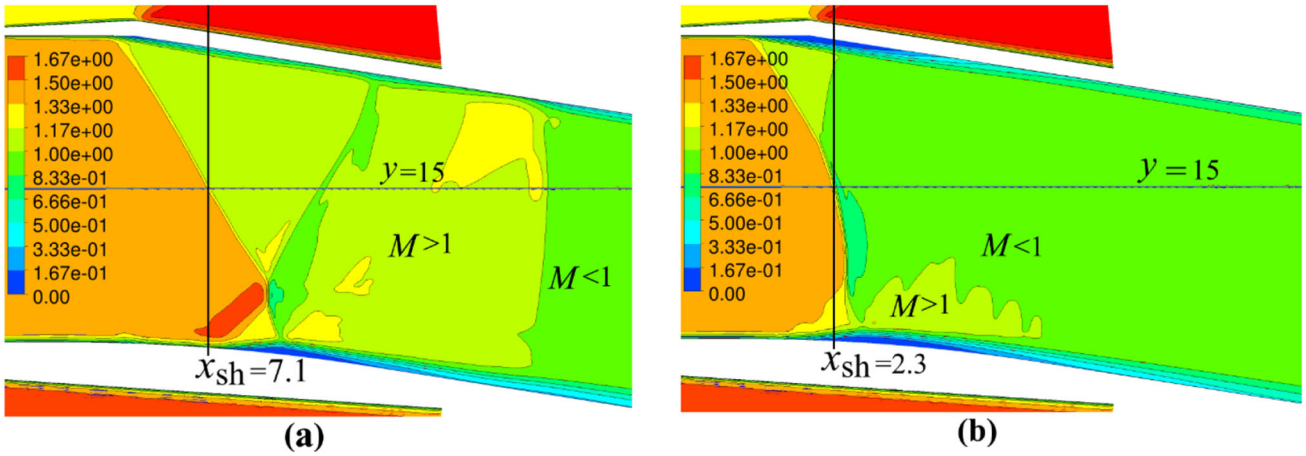

Fig. 4 Mach number contours in Channel A at **a** $M_\infty = 1.585$ and **b** $M_\infty = 1.584$ in the regimes indicated in Fig. 3 by the symbols ▲ and ▼, respectively

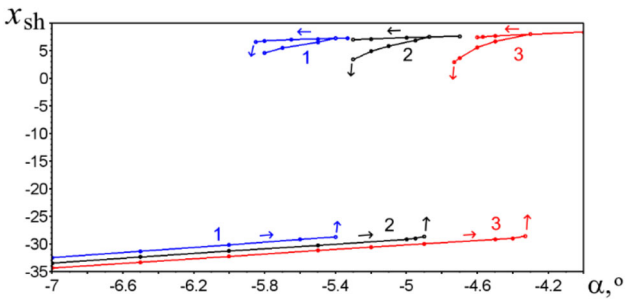

Fig. 5 Channel A: coordinate x_{sh} of shock wave as a function of the angle of attack α at $p_{exit} = 1.82 \times 10^5$ Pa and three Mach numbers: 1—$M_\infty = 1.60$, 2—$M_\infty = 1.59$, 3—$M_\infty = 1.58$

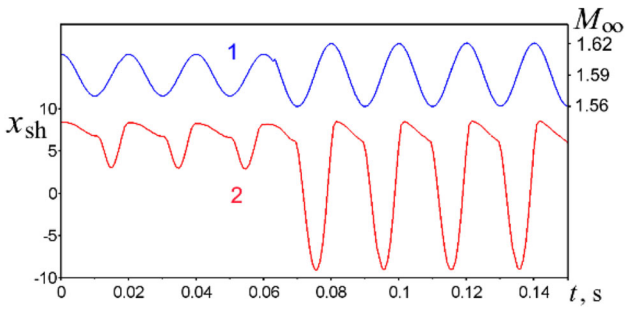

Fig. 6 Channel A: 1—oscillations of M_∞ in time t; 2—shock coordinate x_{sh} obtained by solving problem (1) at $\tau = 0.02$ s and $A = 0.02$ for $t < 0.063$ s, $A = 0.03$ for $t > 0.063$ s

3.2 Oscillatory regimes in Channel A

For a study of the oscillatory regimes, we first set the back-pressure p_{exit} to 1.82×10^5 Pa and impose oscillations of the free-stream Mach number as follows:

$$M_\infty(t) = 1.59 + A\sin(\pi/2 + 2\pi t/\tau),$$
$$\text{initial state : steady flow with a swallowed shock at } M_\infty = 1.59 + A, \quad (1)$$

$$M_\infty(t) = 1.59 + A\sin(-\pi/2 + 2\pi t/\tau),$$
$$\text{initial state : steady flow with an expelled shock at } M_\infty = 1.59 - A. \quad (2)$$

The phases of sine are chosen so as to provide the consistency of boundary and initial conditions. The mid-value 1.59 of $M_\infty(t)$ lies in the hysteresis band where steady flow regimes are non-unique, see curve 1 in Fig. 3. That is why solutions of problems (1) and (2) demonstrate different regimes if A and τ are small enough. Also at $A = 0.02$, $\tau = 0.02$ s, solutions of problems (1) and (2) are different (see curves 2 in Figs. 6 and 7 at $t < 0.063$ s), though the maximum and minimum of $M_\infty(t)$ lie outside of the hysteresis range of

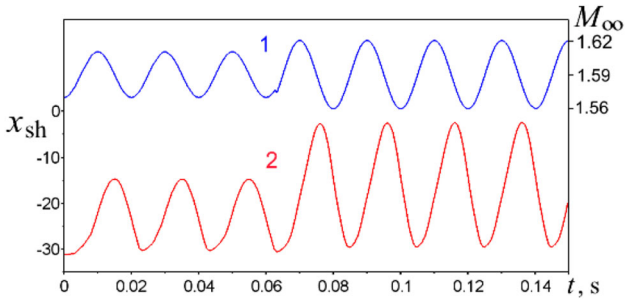

Fig. 7 Channel A: 1—oscillations of M_∞ in time t; 2—shock coordinate x_{sh} obtained by solving problem (2) at $\tau = 0.02$ s and $A = 0.02$ for $t < 0.063$ s, $A = 0.03$ for $t > 0.063$ s

steady flow. An increase in the amplitude A from 0.02 to 0.03 produces larger amplitudes of shock oscillations, as curves 2 in Figs. 6 and 7 show at $t > 0.063$ s, while different oscillatory regimes persist.

The realization of different regimes is explained by the fact that period $\tau = 0.02$ s is insufficiently large for ensuring transitions between upper and lower branches of curve 1 in

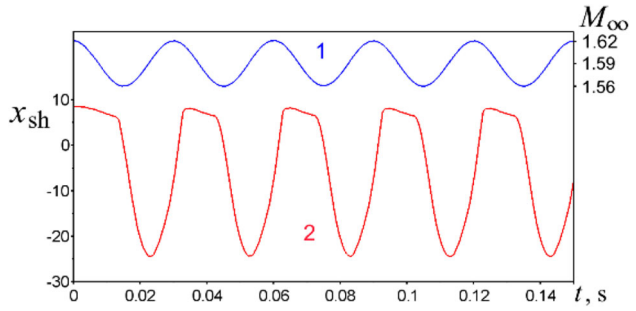

Fig. 8 Channel A: 1—oscillations of M_∞ in time t, 2—shock coordinate x_{sh} obtained by solving problem (1) at $\tau = 0.03$ s, $A = 0.03$

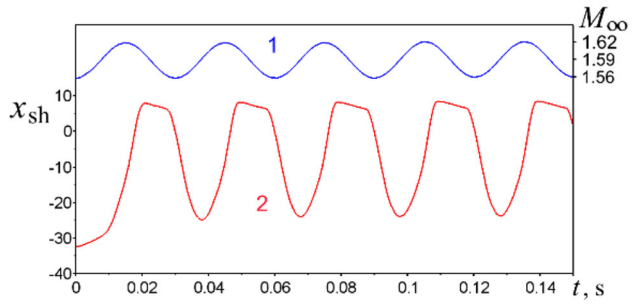

Fig. 9 Channel A: 1—oscillations of M_∞ in time t, 2—shock coordinate x_{sh} obtained by solving problem (2) at $\tau = 0.03$ s, $A = 0.03$

Fig. 3. For example, in the case of problem (1), the time interval of $\tau/2$, in which $M_\infty(t)$ decreases from 1.61 to 1.57, is insufficient for a transition from the regime with a swallowed shock to the regime with an expelled shock. Similarly, in the case of problem (2), the time interval of $\tau/2$, in which $M_\infty(t)$ rises from 1.57 to 1.61, is insufficient for a transition from the regime with an expelled shock to the regime with a swallowed shock.

At the larger period of Mach number oscillations $\tau = 0.03$ s and same amplitude $A = 0.03$, computations showed an expansion of shock oscillations in such a way that the shock location alternates between the entrance and bend sections of channel. This is true for solutions of both problems (1) and (2), which eventually demonstrate oscillations of $x_{sh}(t)$ between − 24.0 and 8.2, see Figs. 8 and 9; the only distinction between the obtained solutions is a shift in time. Further increase in τ or A results in rising the amplitude of shock oscillations.

Now we fix $M_\infty = 1.59$ and impose oscillations of the backpressure p_{exit} as follows:

$$p_{exit}(t) = 1.82 \times 10^5[\text{Pa}] + A\sin(\pi/2 + 2\pi t/\tau), \quad (3)$$

initial state : steady flow with an expelled shock at

$$p_{exit} = 1.82 \times 10^5[\text{Pa}] + A,$$

$$p_{exit}(t) = 1.82 \times 10^5[\text{Pa}] + A\sin(-\pi/2 + 2\pi t/\tau), \quad (4)$$

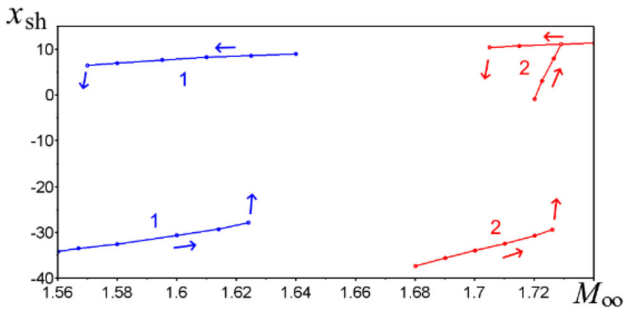

Fig. 10 Channel B: coordinate x_{sh} of shock wave as a function of the steady Mach number M_∞: 1—$p_{exit} = 1.82 \times 10^5$ Pa, 2—$p_{exit} = 2.4 \times 10^5$ Pa

initial state : steady flow with a swallowed shock at

$$p_{exit} = 1.82 \times 10^5[\text{Pa}] - A.$$

The chosen mid-value 1.82×10^5 Pa of p_{exit} lies in a hysteresis band obtained with step-by-step changes in p_{exit} [13, Fig. 11].

Table 1 shows margins of the fully developed oscillations of the shock coordinate x_{sh} at several values of A and τ. As seen, in cases 1 and 2, the shock oscillations obtained by solving problems (3) and (4) occur in different parts of the channel. Meanwhile, an increase in the amplitude A up to 1.2×10^4 Pa (case 3) triggers a transition of the solution of problem (4) to the regime with shock locations near the entrance, and eventually to the coincidence of solutions of both problems. After that, a rise in τ or A only produces expansions of the ranges of oscillations (cases 4, 5).

3.3 Steady and oscillatory flows in Channel B

For Channel B at $p_{exit} = 1.82 \times 10^5$ Pa and step-by-step variation of steady M_∞, the numerical simulation showed hysteresis with only two branches in the dependence $x_{sh}(M_\infty)$, see curve 1 in Fig. 10. The width of hysteresis is six times larger than that obtained for Channel A, as shows a comparison of curves 1 Figs. 3 and 10. Figure 10 demonstrates also a double hysteresis (with three branches of the hysteresis curve 2) at a higher backpressure.

For unsteady free-stream Mach numbers, in order to explore an effect of the amplitude of oscillations, we set the backpressure to 2.4×10^5 Pa and consider the problems:

$$M_\infty(t) = M_{mid} + A\sin(\pi/2 + 2\pi t/\tau), \quad (5)$$

initial state : steady flow with a swallowed shock at $M_\infty = M_{mid} + A$,

$$M_\infty(t) = M_{mid} + A\sin(-\pi/2 + 2\pi t/\tau), \quad (6)$$

initial state : steady flow with an expelled shock at $M_\infty = M_{mid} - A$.

Table 1 Ranges of oscillations of the shock coordinate x_{sh} in Channel A

	Amplitude A, Pa of $p_{exit}(t)$ oscillations	Period τ, s of $p_{exit}(t)$ oscillations	Range obtained by solving problem (3)	Range obtained by solving problem (4)
Case 1	0.8×10^4	0.02	$-30.4 \le x_{sh}(t) \le -20.4$	$2.6 \le x_{sh}(t) \le 7.4$
Case 2	1.0×10^4	0.02	$-31.0 \le x_{sh}(t) \le -19.0$	$-2.35 \le x_{sh}(t) \le 7.4$
Case 3	1.2×10^4	0.02	$-31.4 \le x_{sh}(t) \le -17.6$	$-31.4 \le x_{sh}(t) \le -17.7$
Case 4	1.5×10^4	0.02	$-32.1 \le x_{sh}(t) \le -16.3$	$-32.1 \le x_{sh}(t) \le -16.3$
Case 5	1.5×10^4	0.03	$-32.2 \le x_{sh}(t) \le -9.0$	$-32.2 \le x_{sh}(t) \le -9.0$

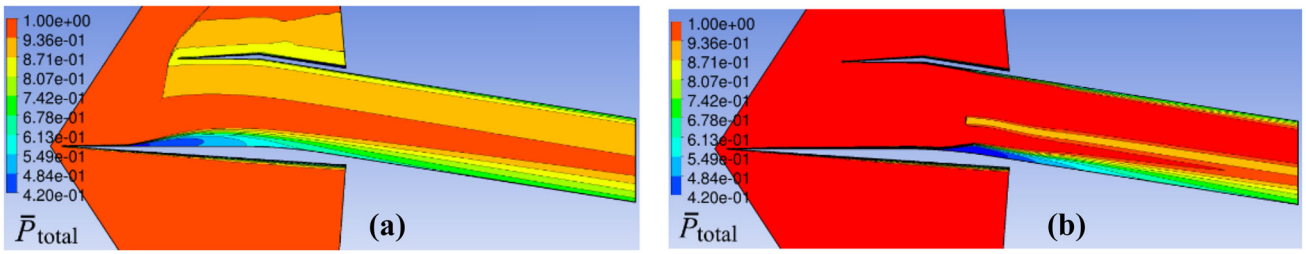

Fig. 11 Channel B: contours of non-dimensional total pressure $\overline{P}_{total}$ when **a** $x_{sh}(t) = -34.3$, **b** $x_{sh}(t) = 11.6$. The flow fields are obtained by solving problems (6) and (5), respectively, at $M_{mid} = 1.72$, $A = 0.03$, $\tau = 0.03$ s

When $A = 0.03$, $\tau = 0.03$ s, and $M_{mid} = 1.72$, shock wave oscillations obtained by solving problems (5) and (6) occur in different parts of channel, at $-11.35 \le x_{sh}(t) \le 11.6$ and $-34.3 \le x_{sh}(t) \le 8.3$, respectively. Figure 11 displays contours of non-dimensional total pressure $\overline{P}_{total} = P_{total}/P_{total,\infty,mid} = P_{total}/4.07 \times 10^5$ [Pa] in different regimes at instants that correspond to $x_{sh} = -34.3$ (expelled shock) and $x_{sh} = 11.6$ (swallowed shock). As seen, losses in the total pressure differ significantly in these cases, though the amplitude, period and mid-value of $M_\infty(t)$ are the same.

An increase in the amplitude A from 0.03 to 0.05 results in rising the amplitude of shock wave oscillations and convergence of solutions of problems (5), (6) to each other at sufficiently large t; both solutions show oscillations of x_{sh} between -35.4 and 12.0.

To demonstrate flow hysteresis with variation of the mid-value M_{mid} of $M_\infty(t)$, we have chosen the smaller values of the backpressure, amplitude, and period: $p_{exit} = 1.82 \times 10^5$ Pa, $A = 0.02$, $\tau = 0.02$ s. Figure 12 shows the obtained hysteresis in the range $1.592 \le M_{mid} \le 1.615$ which is shorter than the one determined by curve 1 in Fig. 10; this range further shortens when the amplitude A increases from 0.02 to 0.03.

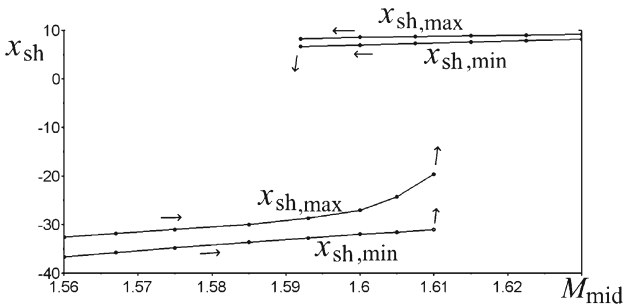

Fig. 12 Channel B: margins of the oscillating shock coordinate $x_{sh,min} \le x_{sh}(t) \le x_{sh,max}$ versus mid-value M_{mid} of Mach number $M_\infty(t)$ at $A = 0.02$, $\tau = 0.02$ s, $p_{exit} = 1.82 \times 10^5$ Pa

4 Conclusion

The numerical simulations revealed non-uniqueness of transonic flow in the short and long 9°-bent channels at small values of the amplitude and period of Mach number $M_\infty(t)$ or backpressure $p_{exit}(t)$ oscillations. Non-unique regimes imply different locations of shock waves in the channels; realization of a certain regime depends on initial conditions. At large amplitudes, the oscillatory flow is unique, and shock location alternates in time between vicinities of the entrance and bent section.

For the long Channel B, the width of flow hysteresis obtained with step-by-step variation of M_∞ is essentially larger than that for Channel A. Gradual variation of the mid-value M_{mid} of the oscillating Mach number $M_\infty(t)$ confirms the existence of hysteresis.

Total pressure losses in non-unique regimes are noticeably different. In practice, different total pressures at the exit of an intake may influence the fuel burning in the combustion chamber and eventually the thrust of engine. Further studies will address non-unique regimes of oscillatory transonic flow in three-dimensional channels and mixed-compression intakes.

Acknowledgements This research was performed using computational resources provided by the Computational Center of St. Petersburg State University (http://cc.spbu.ru).

Funding The work was supported by a grant no. 92211015 from St. Petersburg State University.

Data availability The author declares that the data supporting the findings of this study are available within the paper, and any supplementary information is available from the author on reasonable request.

Declarations

Conflict of interest The author has no relevant financial or non-financial interests to disclose.

References

1. Xie W, Guo R (2008) A ventral diverterless high offset S-shaped inlet at transonic speeds. Chin J Aeronaut 21:207–214. https://doi.org/10.1016/S1000-9361(08)60027-8
2. Das S, Prasad JK (2010) Starting characteristics of a rectangular supersonic air intake with cowl deflection. Aeronaut J 114:177–189. https://doi.org/10.1017/S0001924000003626
3. Bravo-Mosquera PD, Abdalla AM, Cerón-Muñoz HD, Catalano FM (2018) Design and performance assessment of an inverted rectangular dorsal intake for military aviation. In: 31st Congress of the Int. Council of the Aeronautical Sciences. Sept. 9–14, 2018, Belo Horizonte, ICAS2018–0814, 1–14
4. Han JA, Zhong JJ, Yan HM, Sun P, Yu Y (2009) Numerical research of three dimensional flow-path in a ram-rotor. J Aerosp Power 24(5):1079–1088. http://caod.oriprobe.com/articles/17247810/Numerical_research_of_three_dimensional_flow_path_in_a_ram_rotor.htm
5. Kang W, Liu Zh, Lu J, Wang Y, Dong Y (2014) A numerical study for flow excitation and performance of rampressor inlet considering rotor motion. Shock Vib 2014:963234. https://doi.org/10.1155/2014/963234
6. Guo S, Wang Z, Zhao Y (2014) The flow hysteresis in the supersonic curved channel. J Natl Univ Def Technol 36(4):10–14
7. Feng S, Chang J, Zhang Ch, Wang Y, Ma J, Bao W (2017) Experimental and numerical investigation on hysteresis characteristics and formation mechanism for a variable geometry dual-mode combustor. Aerosp Sci Technol 67:96–104. https://doi.org/10.1016/j.ast.2017.03.040
8. Feng S, Chang J, Zhang Y, Zhang Ch, Wang Y, Bao W (2017) Numerical studies for performance improvement of a variable geometry dual mode combustor by optimizing deflection angle. Aerosp Sci Technol 68:320–330. https://doi.org/10.1016/j.ast.2017.05.025
9. KrushnaraoKotteda VM, Mittal S (2016) Flow in a Y-intake at supersonic speeds. J Propuls Power 32(1):171–187
10. Jin Y, Sun S, Tan H, Zhang Y, Huang H (2022) Flow response hysteresis of throat regulation process of a two-dimensional mixed-compression supersonic inlet. Chin Aeronaut 35(3):112–127. https://doi.org/10.1016/j.cja.2021.06.013
11. Kuzmin A, Babarykin K (2018) Supersonic flow bifurcation in twin intake models. Adv Aircr Spacecr Sci 5(4):445–458. https://doi.org/10.12989/aas.2018.5.4.445
12. Kuzmin A (2019) Shock wave instability in a bent channel with subsonic/supersonic exit. Adv Aircr Spacecr Sci 6(1):19–30. https://doi.org/10.12989/aas.2019.6.1.019
13. Kuzmin A (2019) Non-uniqueness of transonic flow in an intake-type channel. J Phys Conf Ser 1392:012012. https://doi.org/10.1088/1742-6596/1392/1/012012
14. Tennekes H, Lumley JL (1992) A first course in turbulence, 14th edn. MIT Press, Cambridge
15. ANSYS Fluids (2023) Computational fluid dynamics. https://www.ansys.com/products/fluids. Accessed 18 Apr 2023
16. Menter FR (2009) Review of the shear-stress transport turbulence model experience from an industrial perspective. Int J Comput Fluid Dyn 23:305–316. https://doi.org/10.1080/10618560902773387
17. Suryan A, Shin ChS, Setoguchi T, Kim HD (2010) Visualization of hysteresis phenomenon of shock waves in supersonic internal flow. J Korean Soc Vis 8(2):31–39. https://doi.org/10.5407/JKSV.2010.8.2.031
18. Huang T, Yue L, Ma S, Zhang Q, Zhang P, Chang X (2020) Numerical investigation on flow nonuniformity-induced hysteresis in scramjet isolator. Chin J Aeronaut 33:3176–3188. https://doi.org/10.1016/j.cja.2020.04.019